ARQII Publication
http://arqiipubl.com/ams
APPLICATIONS OF
MODELLING AND SIMULATION
eISSN 2600-8084
VOL 8, 2024, 70-77

Porous Functionally Graded Circular Plate with an Uneven Porosity Distribution in the Thermal Environment

Lan Hoang Ton That*

Faculty of Civil Engineering, HCMC University of Architecture, Ho Chi Minh City, Vietnam

*Corresponding author: tonthathoanglan.247@gmail.com

Submitted 28 October 2023, Revised 13 March 2024, Accepted 28 March 2024, Available online 16 April 2024.

Abstract: Functionally graded materials are commonly used in thermal environments to change the properties of constituent materials. Besides the outstanding advantages, there are still disadvantages related to the manufacturing process, such as internal porosity, that affect the mechanical properties of this material. The purpose of this paper is to shed light on how a porous, functionally graded circular plate with an uneven porosity distribution behaves when heated. This work provides a numerical method for this structure based on a type of C^0-HSDT (higher-order shear deformation theory) coupled to Shi's third-order shear deformation theory. Without the shear correction factor, Shi's theory has the desirable properties and advantages of a third-order shear deformation theory. It is assumed that a uniform temperature distribution is demonstrated across the thickness of this structure, and then numerical solutions are given to verify the accuracy of this proposed process.

Keywords: Circular plate; Finite element analysis; Porous functionally graded material; Thermal environment; Uneven porosity distribution.

1. INTRODUCTION

Functionally graded materials have been successfully applied in numerous fields of engineering. The material is normally made from a mixture of ceramic and metal and provides continuous variation in material properties from the bottom surface to the top surface of the plate. Functionally graded materials have received more attention in thermal environments such as spacecraft, nuclear tanks, and so on. The analytical solutions [1–4] are valuable in some cases, but in general, with complicated geometries or complex conditions like high temperatures in thermal environments, etc., they are often limited. It is easily recognized that the third-order shear deformation plate theories are the most effective and accurate theories due to the quadratic variation of the transverse shear strains and stresses along the thickness of the plate, as well as the shear locking free. Recently, Shi [5] gave a simple third-order shear deformation plate theory based on rigorous kinematics of displacements, initially applied to the static analysis of isotropic and orthotropic beams and plates. The solutions obtained by Shi's theory have been indicated to be more reliable and highly accurate than others. Beside the analytical approaches, numerical methods are used in the structural analyses [6–12], etc.

In literature [6], based on the three-dimensional elasticity theory, the transient thermal residual stress analyses of one-dimensional functionally graded rectangular plates have been performed under in-plane constant heat flux for different compositional gradient exponents. The thermo-mechanical properties were assumed to vary with a power law along an in-plane direction, not through the plate thickness direction, and were temperature-dependent/independent. The heat transfer and Navier's equations in cartesian coordinates, which represent the two-dimensional thermoelastic problem, were resolved by means of the finite-difference method, and the set of linear equations was solved using the pseudo-singular value method. The effect of the coordinate derivatives of material properties was considered in both heat transfer and Navier's equations. In paper [7], the geometrically nonlinear static response of a functionally graded piezoelectric plate under mechanical and electrical loads was studied using the mesh-less method. The radial point interpolation method was used to create the shape function and approximate the field variables. The first-order shear deformation plate theory and Von Karman strains were used to model the nonlinear behavior of the plate. Power law distribution through the thickness was considered for all mechanical and piezoelectric properties. The Newton-Raphson method was used to solve the obtained nonlinear coupled equations. The static and dynamic analysis of functionally graded material skew plates under mechanical load was studied. The finite element method (FEM) formulation, based on a third-order shear deformation theory that did not require any shear correction factor,

was used in [8]. The C^1 continuity requirement of the higher-order theory was overcome in this study by adopting a C^0 continuous isoparametric Lagrangian element with seven degrees of freedom at each node. The Mori-Tanaka homogenization scheme was used to estimate the effective properties of the constituents, and it was assumed that mechanical properties vary according to a power-law distribution of the volume fraction of the constituents. The effects of skew angle, boundary conditions, volume-fraction exponent, loading conditions, aspect ratio, thickness ratio, and other parameters on deflection, natural frequency, and critical buckling load of functionally graded skew plates were reported, which could serve as a benchmark for another research.

In [9], the free vibration of functionally graded nonuniform straight-sided plates with circular and non-circular cutouts was investigated. Moreover, thermal effects on free vibration analysis and the effects of various parameters on the natural frequencies of these plates were evaluated. The material properties were assumed to be graded across thicknesses, which vary according to the linear distribution law. The investigated parameters were cutout size, type of loading, and different boundary conditions. A nonlinear finite element model was proposed in [10] to study the dynamic response of functionally graded material plates subjected simultaneously to thermal, static, and harmonic loads. The material properties depended on the temperature and were assumed to vary continuously in the thickness direction according to a simple power law distribution. The third-order shear deformation theory of Reddy was modified for functionally graded material (FGM) plates by considering the physical/exact neutral surface. Extended Hamilton's principle was used to obtain the equations of motion in structural nodes degree of freedom. Using the exact neutral surface in equations of motion, the in-plane and out-of-plane motions of FGM plates could be separated, similar to homogenous plates. The order of the equations of motion was reduced using the modal reduction method. The shooting method was used to obtain the initial conditions for a periodic response. Three bucked equilibrium positions were obtained for FGM plates with immovable boundaries under thermal load. The new numerical procedure for functionally graded skew plates in a thermal environment was presented in [11] based on the C^0-form of the novel third-order shear deformation theory. Without the shear correction factor, this theory was also taking advantage of the desirable properties and advantages of the third-order shear deformation theory. The uniform distribution of temperature was embedded across the thickness of the plate. Both the rule of mixture and the micromechanics approaches were considered to describe the variation of material compositions across the thickness. A thermo-elastic contact problem of functionally graded materials rotating brake disks with different pure brake pad areas under temperature-dependent material properties was solved by the FEM. The properties of brake disks changed gradually from metal to ceramic by power-law distribution along the radial direction from the inner to the outer surface. Areas of the pure pad were changing while the vertical force was constant. The ratio of brake pad thickness to FGM brake disk thickness was assumed to be 0.66. Two sources of thermal loads were considered: (1) heat generation between the pad and brake disk due to contact friction; and (2) external thermal load due to a constant temperature at the inner and outer surfaces. The mechanical responses of the FGM disk were compared with several pad contact areas. The results for temperature-dependent and temperature-independent material properties were investigated and presented in the literature [12].

The main goal of this work, in a different way from previous research, is to use Shi's third-order shear deformation theory to apply C^0-form finite element analysis to the thermal environment of a porous functionally graded circular plate. This study examines the impact of porosity within the structure on the deflection value. The effective characteristics were considered to be temperature-dependent when conducting numerical analysis. Furthermore, the C^0-HSDT (higher-order shear deformation theory) model provided results without needing shear-correct factors. It is also noticed that the quadrilateral element associated with the C^0-HSDT only uses bilinear function approximations and does not require a high computational cost.

The next sections of this paper are given as follows: The concept of FGM, including an uneven porosity distribution, the change of material properties under thermal conditions, and the finite element formulation for static analysis, is presented in Section 2. The numerical solutions of static bending deflections are shown in Section 3. Some concluding remarks are given in the last section.

2. POROUS FUNCTIONALLY GRADED CIRCULAR PLATE AND FINITE ELEMENT FORMULATION

A porous functionally graded circular plate is plotted in Figure 1. The mid-plane of the plate is the *xy*-plane, while the *z*-axis is perpendicular to the *xy*-plane.

The volume fraction of the ceramic (V_c) and the metal (V_m) are described as

$$V_c = \left(\frac{z}{t}+\frac{1}{2}\right)^n;\ V_m = 1 - V_c \text{ with } n \geq 0 \tag{1}$$

where t is the thickness of plate, z is the thickness coordinate variable with $-t/2 \leq z \leq t/2$ as well as c, m, n and e represent the ceramic and metal constituents, the non-negative volume fraction gradient index, and the coefficient of porosity, respectively. The values of material properties $M(z)$ are formulated and then depicted in Figure 2 for Young's modulus E as an example.

$$M(z) = M_m + (M_c - M_m)\left(\frac{1}{2}+\frac{z}{t}\right)^n - (M_c + M_m)\frac{e}{2}\left(1 - \frac{2|z|}{t}\right) \tag{2}$$

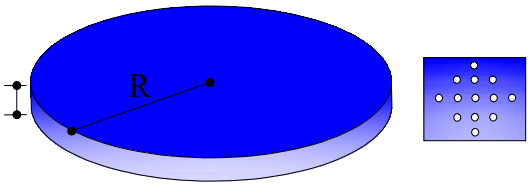

Figure 1. The porous functionally graded circular plate with an uneven porosity distribution.

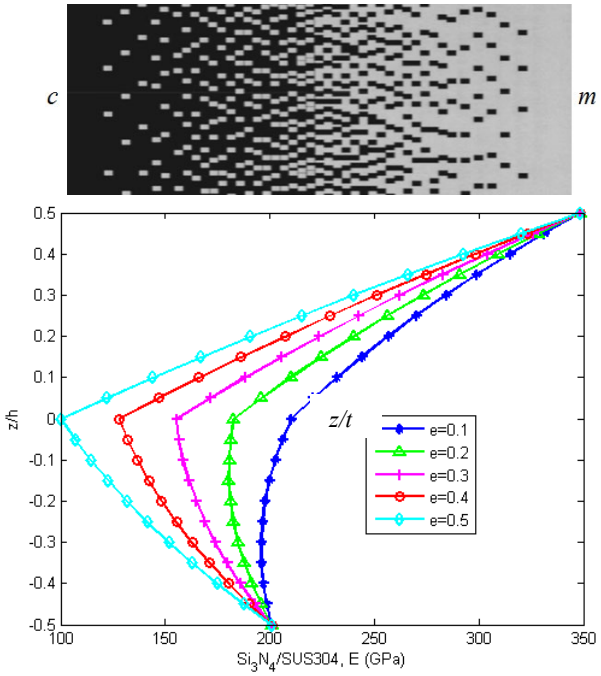

Figure 2. The illustration of functionally graded material and modification of E under varying e.

The function of temperature $T(K)$ can be expressed as [1]

$$P = P_0\left(P_{-1}T^{-1} + 1 + P_1T + P_2T^2 + P_3T^3\right) \tag{3}$$

where $T = T_0 + \Delta T$ and $T_0 = 300$ K (ambient or free stress temperature), ΔT is the temperature change, and P_0, P_{-1}, P_1, P_2, P_3 are the coefficients of temperature $T(K)$, and are unique to each constituent. According to the theory of Shi [5], the three-dimensional displacement field (u, v, w) can be expressed in terms of C^0-HSDT and seven unknown variables as follows:

$$u(x,y,z) = u_0(x,y) + \left(\frac{1}{4}z - \frac{5}{3t^2}z^3\right)\phi_x^b + \frac{5}{4}\left(z - \frac{4}{3t^2}z^3\right)\phi_x^s(x,y) \tag{4}$$

$$v(x,y,z) = v_0(x,y) + \left(\frac{1}{4}z - \frac{5}{3t^2}z^3\right)\phi_y^b + \frac{5}{4}\left(z - \frac{4}{3t^2}z^3\right)\phi_y^s(x,y) \tag{5}$$

$$w(x,y,z) = w_0(x,y) \tag{6}$$

with seven unknowns including three axial and transverse displacements and four rotations. The strain-displacement relations can be given in a matrix form as

$$\begin{Bmatrix}\boldsymbol{\varepsilon}\\ \boldsymbol{\gamma}\end{Bmatrix} = \begin{Bmatrix}\boldsymbol{\varepsilon}^{(0)}\\ \boldsymbol{\gamma}^{(0)}\end{Bmatrix} + z\begin{Bmatrix}\boldsymbol{\varepsilon}^{(1)}\\ \mathbf{0}\end{Bmatrix} + z^2\begin{Bmatrix}\mathbf{0}\\ \boldsymbol{\gamma}^{(2)}\end{Bmatrix} + z^3\begin{Bmatrix}\boldsymbol{\varepsilon}^{(3)}\\ \mathbf{0}\end{Bmatrix} \tag{7}$$

with

$$\boldsymbol{\varepsilon}^{(0)} = \begin{Bmatrix} u_{0,x} \\ v_{0,y} \\ u_{0,y} + v_{0,x}\end{Bmatrix};\ \boldsymbol{\varepsilon}^{(1)} = \frac{1}{4}\begin{Bmatrix} \left(5\phi_{x,x}^s + \phi_{x,x}^b\right) \\ \left(5\phi_{y,y}^s + \phi_{y,y}^b\right) \\ \left(5\phi_{x,y}^s + 5\phi_{y,x}^s + \phi_{x,y}^b + \phi_{y,x}^b\right)\end{Bmatrix};\ \boldsymbol{\varepsilon}^{(3)} = \frac{-5}{3t^2}\begin{Bmatrix} \phi_{x,x}^s + \phi_{x,x}^b \\ \phi_{y,y}^s + \phi_{y,y}^b \\ \phi_{x,y}^s + \phi_{x,y}^b + \phi_{y,x}^s + \phi_{y,x}^b\end{Bmatrix} \tag{8}$$

$$\boldsymbol{\gamma}^{(0)} = \begin{Bmatrix} \frac{5}{4}\phi_y^s + \frac{1}{4}\phi_y^b + w_{,y} \\ \frac{5}{4}\phi_x^s + \frac{1}{4}\phi_x^b + w_{,x}\end{Bmatrix};\ \boldsymbol{\gamma}^{(2)} = \frac{-5}{t^2}\begin{Bmatrix}\phi_y^s + \phi_y^b \\ \phi_x^s + \phi_x^b\end{Bmatrix} \tag{9}$$

The constitutive equation is expressed as

$$\boldsymbol{\sigma} = \mathbf{D}_m(\mathbf{z})(\boldsymbol{\varepsilon}^{(0)} + \mathbf{z}\boldsymbol{\varepsilon}^{(1)} + \mathbf{z}^3\boldsymbol{\varepsilon}^{(3)} - \boldsymbol{\varepsilon}^{(T)}) \tag{10}$$

$$\boldsymbol{\tau} = \mathbf{D}_s(z)\left(\boldsymbol{\gamma}^{(0)} + \mathbf{z}^2\boldsymbol{\gamma}^{(2)}\right) \tag{11}$$

in which

$$\boldsymbol{\sigma} = \begin{bmatrix}\sigma_x & \sigma_y & \sigma_{xy}\end{bmatrix}^{\mathrm{T}};\ \boldsymbol{\tau} = \begin{bmatrix}\tau_{yz} & \tau_{xz}\end{bmatrix}^{\mathrm{T}} \tag{12}$$

$$\mathbf{D}_m(z) = \frac{E(z)}{1-v(z)^2}\begin{bmatrix}1 & v(z) & 0\\ v(z) & 1 & 0\\ 0 & 0 & (1-v(z))/2\end{bmatrix} \tag{13}$$

$$\mathbf{D}_s(z) = \frac{E(z)}{2(1+v(z))}\begin{bmatrix}1 & 0\\ 0 & 1\end{bmatrix} \tag{14}$$

$$\boldsymbol{\varepsilon}^{(T)} = \begin{bmatrix}\boldsymbol{\varepsilon}_x^{(T)} & \boldsymbol{\varepsilon}_y^{(T)} & 0\end{bmatrix}^{\mathrm{T}} = \begin{bmatrix}\alpha(z)\Delta T & \alpha(z)\Delta T & 0\end{bmatrix}^{\mathrm{T}} \tag{15}$$

The generalized displacements can hence be approximated as

$$\mathbf{u}_0 = \mathbf{N}\mathbf{q}_e \tag{16}$$

with

$$\mathbf{u}_0 = \begin{bmatrix}u_0 & v_0 & w & \phi_x^s & \phi_y^s & \phi_x^b & \phi_y^b\end{bmatrix}^{\mathrm{T}};\ \mathbf{N} = \begin{bmatrix}N_1 & N_2 & N_3 & N_4\end{bmatrix};\ \mathbf{q}_e = \begin{bmatrix}\mathbf{q}_{1e} & \mathbf{q}_{2e} & \mathbf{q}_{3e} & \mathbf{q}_{4e}\end{bmatrix}^{\mathrm{T}} \tag{17}$$

$\mathbf{q}_e$ and $\mathbf{N}$ are the unknown displacement vector and the shape function vector. The strain can be rewritten as

$$\boldsymbol{\varepsilon} = \left(\mathbf{B}_1 + \mathbf{B}_2 + \mathbf{B}_3\right)\mathbf{q}_e \tag{18}$$

$$\boldsymbol{\gamma} = \left(\mathbf{B}_4 + \mathbf{B}_5\right)\mathbf{q}_e \tag{19}$$

in which

$$\mathbf{B}_1 = \sum_{i=1}^{4}\begin{bmatrix}\mathbf{N}_{i,x} & 0 & 0 & 0 & 0 & 0 & 0\\ 0 & \mathbf{N}_{i,y} & 0 & 0 & 0 & 0 & 0\\ \mathbf{N}_{i,y} & \mathbf{N}_{i,x} & 0 & 0 & 0 & 0 & 0\end{bmatrix};\ \mathbf{B}_2 = \frac{1}{4}\sum_{i=1}^{4}\begin{bmatrix}0 & 0 & 0 & 5\mathbf{N}_{i,x} & 0 & \mathbf{N}_{i,x} & 0\\ 0 & 0 & 0 & 0 & 5\mathbf{N}_{i,y} & 0 & \mathbf{N}_{i,y}\\ 0 & 0 & 0 & 5\mathbf{N}_{i,y} & 5\mathbf{N}_{i,x} & \mathbf{N}_{i,y} & \mathbf{N}_{i,x}\end{bmatrix} \tag{20}$$

$$\mathbf{B}_3 = -\frac{5}{3t^2}\sum_{i=1}^{4}\begin{bmatrix}0 & 0 & 0 & \mathbf{N}_{i,x} & 0 & \mathbf{N}_{i,x} & 0\\ 0 & 0 & 0 & 0 & \mathbf{N}_{i,y} & 0 & \mathbf{N}_{i,y}\\ 0 & 0 & 0 & \mathbf{N}_{i,y} & \mathbf{N}_{i,x} & \mathbf{N}_{i,y} & \mathbf{N}_{i,x}\end{bmatrix} \tag{21}$$

$$\mathbf{B}_4 = \sum_{i=1}^{4}\begin{bmatrix}0 & 0 & \mathbf{N}_{i,y} & 0 & \frac{5}{4} & 0 & \frac{1}{4}\\ 0 & 0 & \mathbf{N}_{i,x} & \frac{5}{4} & 0 & \frac{1}{4} & 0\end{bmatrix};\ \mathbf{B}_5 = -\frac{5}{t^2}\sum_{i=1}^{4}\begin{bmatrix}0 & 0 & 0 & 0 & 1 & 0 & 1\\ 0 & 0 & 0 & 1 & 0 & 1 & 0\end{bmatrix} \tag{22}$$

The normal forces, bending moments, higher-order moments and shear force can then be computed through the following relations.

$$\begin{Bmatrix}\bar{\mathbf{N}}\\ \bar{\mathbf{M}}\\ \bar{\mathbf{P}}\\ \bar{\mathbf{Q}}\\ \bar{\mathbf{R}}\end{Bmatrix} = \begin{bmatrix}\bar{\mathbf{A}} & \bar{\mathbf{B}} & \bar{\mathbf{E}} & \mathbf{0} & \mathbf{0}\\ \bar{\mathbf{B}} & \bar{\mathbf{D}} & \bar{\mathbf{F}} & \mathbf{0} & \mathbf{0}\\ \bar{\mathbf{E}} & \bar{\mathbf{F}} & \bar{\mathbf{H}} & \mathbf{0} & \mathbf{0}\\ \mathbf{0} & \mathbf{0} & \mathbf{0} & \hat{\mathbf{A}} & \hat{\mathbf{B}}\\ \mathbf{0} & \mathbf{0} & \mathbf{0} & \hat{\mathbf{B}} & \hat{\mathbf{D}}\end{bmatrix}\begin{Bmatrix}\boldsymbol{\varepsilon}^{(0)}\\ \boldsymbol{\varepsilon}^{(1)}\\ \boldsymbol{\varepsilon}^{(3)}\\ \boldsymbol{\gamma}^{(0)}\\ \boldsymbol{\gamma}^{(2)}\end{Bmatrix} - \begin{Bmatrix}\bar{\mathbf{N}}^{(T)}\\ \bar{\mathbf{M}}^{(T)}\\ \bar{\mathbf{P}}^{(T)}\\ \mathbf{0}\\ \mathbf{0}\end{Bmatrix} \tag{23}$$

with

$$\left(\bar{\mathbf{A}},\ \bar{\mathbf{B}},\ \bar{\mathbf{D}},\ \bar{\mathbf{E}},\ \bar{\mathbf{F}},\ \bar{\mathbf{H}}\right) = \int_{-t/2}^{t/2}\left(1,\ z,\ z^2,\ z^3,\ z^4,\ z^6\right)\mathbf{D}_m(z)dz \tag{24}$$

$$\left(\hat{\mathbf{A}},\ \hat{\mathbf{B}},\ \hat{\mathbf{D}}\right) = \int_{-t/2}^{t/2}\left(1,\ z^2,\ z^4\right)\mathbf{D}_s(z)dz \tag{25}$$

$$\left(\bar{\mathbf{N}}^{(T)},\ \bar{\mathbf{M}}^{(T)}, \bar{\mathbf{P}}^{(T)}\right) = \int_{-t/2}^{t/2}\mathbf{D}_m(z)\left(1,\ z,\ z^3\right)\{1\ \ 1\ \ 0\}^{\mathrm{T}}\,\alpha(z)\Delta T dz \tag{26}$$

The total strain energy of a plate due to the normal forces, shear force, bending moments and higher-order moments can be given by

$$U = \frac{1}{2}\int_{V_e} \boldsymbol{\varepsilon}^{\mathrm{T}}\boldsymbol{\sigma} dV - \int_{S_e} \mathbf{u}^{\mathrm{T}}\mathbf{f} dS = \frac{1}{2}\mathbf{q}_e^{\mathrm{T}}\int_{S_e} \Upsilon dS \mathbf{q}_e - \mathbf{q}_e^{\mathrm{T}}\int_{S_e} \Psi dS - \mathbf{q}_e^{\mathrm{T}}\int_{S_e} \mathbf{N}^{\mathrm{T}}\mathbf{f} dS + \frac{1}{2}\int_{S_e} \left(\boldsymbol{\varepsilon}^{(T)}\right)^{\mathrm{T}} \bar{\mathbf{A}}\boldsymbol{\varepsilon}^{(T)} dS \tag{27}$$

$$U = \frac{1}{2}\mathbf{q}_e^{\mathrm{T}}\mathbf{K}_e\mathbf{q}_e - \mathbf{q}_e^{\mathrm{T}}\mathbf{F}_e^{(T)} - \mathbf{q}_e^{\mathrm{T}}\mathbf{F}_e + \mathbf{C}^{(T)} = \mathbf{q}_e^{\mathrm{T}}\left(\frac{1}{2}\mathbf{K}_e\mathbf{q}_e - \mathbf{F}_e^{(T)} - \mathbf{F}_e\right) + \mathbf{C}^{(T)} \tag{28}$$

in which

$$\begin{aligned}\Upsilon = {} & \mathbf{B}_1^{\mathrm{T}}\bar{\mathbf{A}}\mathbf{B}_1 + \mathbf{B}_1^{\mathrm{T}}\bar{\mathbf{B}}\mathbf{B}_2 + \mathbf{B}_1^{\mathrm{T}}\bar{\mathbf{E}}\mathbf{B}_3 + \mathbf{B}_2^{\mathrm{T}}\bar{\mathbf{B}}\mathbf{B}_1 + \mathbf{B}_2^{\mathrm{T}}\bar{\mathbf{D}}\mathbf{B}_2 + \mathbf{B}_2^{\mathrm{T}}\bar{\mathbf{F}}\mathbf{B}_3 + \mathbf{B}_3^{\mathrm{T}}\bar{\mathbf{E}}\mathbf{B}_1 \\ & + \mathbf{B}_3^{\mathrm{T}}\bar{\mathbf{F}}\mathbf{B}_2 + \mathbf{B}_3^{\mathrm{T}}\bar{\mathbf{H}}\mathbf{B}_3 + \mathbf{B}_4^{\mathrm{T}}\hat{\mathbf{A}}\mathbf{B}_4 + \mathbf{B}_4^{\mathrm{T}}\hat{\mathbf{B}}\mathbf{B}_5 + \mathbf{B}_5^{\mathrm{T}}\hat{\mathbf{B}}\mathbf{B}_4 + \mathbf{B}_5^{\mathrm{T}}\hat{\mathbf{D}}\mathbf{B}_5\end{aligned} \tag{29}$$

$$\Psi = \mathbf{B}_1^{\mathrm{T}}\bar{\mathbf{N}}^{(T)} + \mathbf{B}_2^{\mathrm{T}}\bar{\mathbf{M}}^{(T)} + \mathbf{B}_3^{\mathrm{T}}\bar{\mathbf{P}}^{(T)} \tag{30}$$

$\mathbf{C}^{(T)}$ disappears and eventually does not present in the final system of discrete equations. The bending solutions can be obtained by solving Equation (31).

$$\mathbf{Kd} = \mathbf{F} + \mathbf{F}^{(T)} \tag{31}$$

3. NUMERICAL SOLUTIONS

The numerical solutions for static bending analysis of porous functionally graded circular plates in a thermal environment are presented. Table 1 gives the different material properties [1, 3], such as Si_3N_4, ZrO_2, and SUS304. To verify the correctness of this procedure on the functionally graded plate in a thermal environment, the temperature under consideration is set to be $T = 300^{\circ}\mathrm{K}$ $(\Delta T = 0)$. The square structure, fully simply supported and made of Si_3N_4/SUS304, is tested. The central deflections can be obtained by $\bar{w} = \left[100 w_c E_m t^3\right] / \left[12\left(1 - v_m^2\right) P a^4\right]$ and compared with the analytical solutions of Wattanasakulpong *et al*. [1] in Table 2. The results reported in this table account for different values of the volume fraction coefficient *n*. As expected, the present numerical results show good agreement with the analytical solutions for each value of *n*. Moreover, as the plate becomes more and more metallic (i.e., the value of *n* increases), the normalized deflection gradually increases.

Next, a fully clamped porous functionally graded circular plate made of Si_3N_4/SUS304 or ZrO_2/SUS304 subjected to a uniform load, *P* is studied. The maximum central deflection of this structure is respectively normalised by $\bar{w} = \left[100 w_c E_m t^3\right] / \left[12\left(1 - v_m^2\right) P R^4\right]$. The influence of the coefficient of porosity, *e* on the mechanical deflection is studied and depicted in Figures 3-6. By completing it, various values of *R/t, n,* and *T* are used to calculate the deflections. For Figure 3(a), corresponding to material Si_3N_4/SUS304, increasing the temperature *T* will increase the deflection value, and this is even more clearly shown when increasing the value of *n* at the same time. In addition, corresponding to Figure 3(b), the appearance of porosity *e* in the structure further increases the deflection, and this observation is still maintained with different *n* values. On the other hand, the numerical results of the dimensionless deflections of the ZrO_2/SUS304 plate show that they first increase and then decrease with increasing the volume fraction exponent, and the transition point occurs at appropriately *T* = 1000 K, and beyond that range, the deflections behave oppositely (Figures 4(a) and 4(b)). Similarly, for Figures 5 and 6, corresponding to the two material groups Si_3N_4/SUS304 and ZrO_2/SUS304, changing the plate thickness *t* (*R*/25, *R*/20, *R*/15, *R*/10 and *R*/5) as well as the *n* or *e* value clearly shows the change in deflection value.

Table 1. Temperature dependent coefficient of Young's modulus *E* (Pa), thermal expansion coefficient α (1/K), Poisson's ratio ν, mass density ρ (kg/m^3) for various materials.

Ceramic/Metal	P_0	P_{-1}	P_1	P_2	P_3	P (300 K)
			Si_3N_4			
E (Pa)	348.43e9	0	-3.070e-4	2.160e-7	-8.946e-11	322.27e9
α (1/K)	5.8723e-6	0	9.095e-4	0	0	7.475e-6
ν	0.24	0	0	0	0	0.240
ρ (kg/m^3)	2370	0	0	0	0	2370
			ZrO_2			
E (Pa)	244.27e9	0	-1.371e-3	1.214e-6	-3.681e-10	168.06e9
α (1/K)	12.766e-6	0	-1.491e-3	1.006e-5	-6.778e-11	18.591e-6
ν	0.288	0	1.133e-4		0	0.298
ρ (kg/m^3)	3657	0	0		0	3657
			SUS304			
E (Pa)	201.04e9	0	3.079e-4	-6.534e-7	0	207.79e9
α (1/K)	12.330e-6	0	8.086e-4	0	0	15.321e-6
ν	0.326	0	-2.002e-4	3.797e-7	0	0.318
ρ (kg/m^3)	8166	0	0	0	0	8166

Table 2. The comparison of normalized deflections for various values of n.

$\bar{w}$							
n=0.5		n=1		n=5		n=10	
[1]	Paper	[1]	Paper	[1]	Paper	[1]	Paper
0.325	0.3248	0.343	0.3464	0.380	0.3847	0.396	0.3998

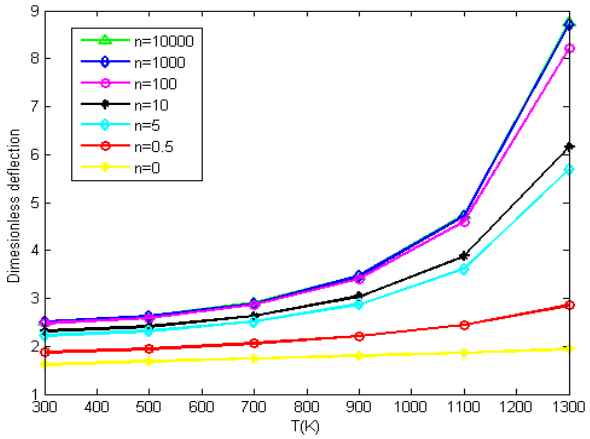

(a) $t = R/10, e = 0$

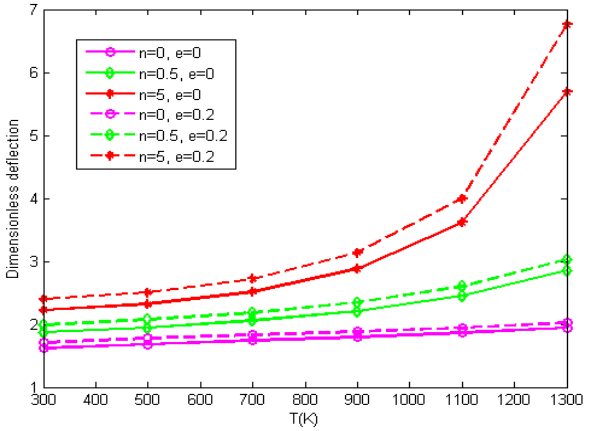

(b) $t = R/10$, $e = 0$, 0.2

Figure 3. Influence of n and T on the dimensionless deflections of a fully clamped Si_3N_4/SUS304 circular plate.

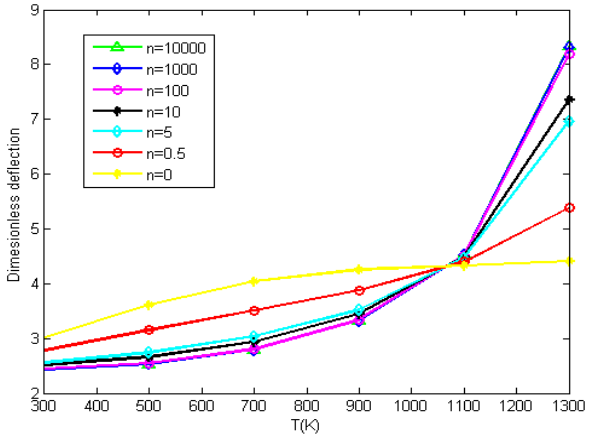

(a) $t = R/10$, $e = 0$

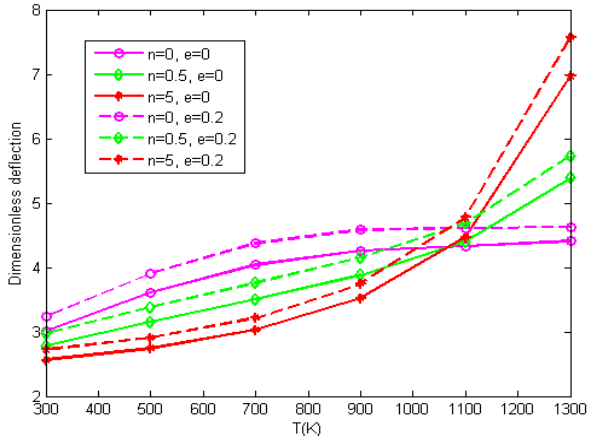

(b) $t = R/10$, $e = 0$, 0.2

Figure 4. Influence of n and T on the dimensionless deflections of a fully clamped ZrO_2/SUS304 circular plate.

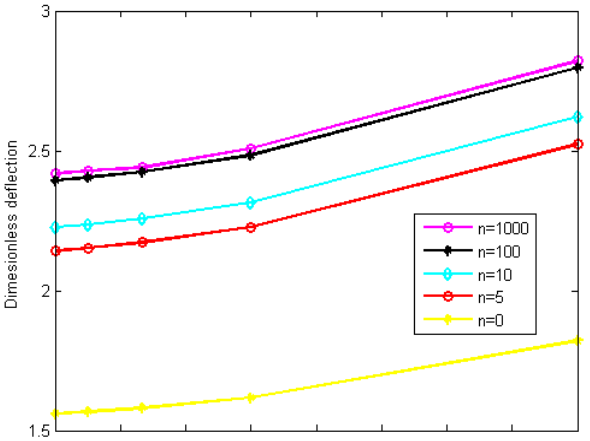

(a) $T = 300$ K, $e = 0$

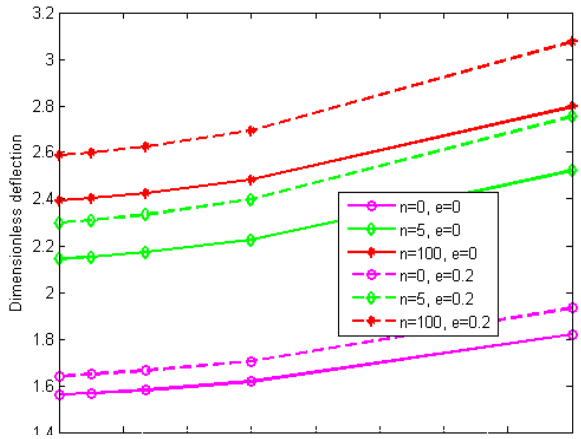

(b) $T = 300$ K, $e = 0$, 0.2

Figure 5. Influence of n and thickness t on the dimensionless deflections of a fully clamped Si_3N_4/SUS304 circular plate.

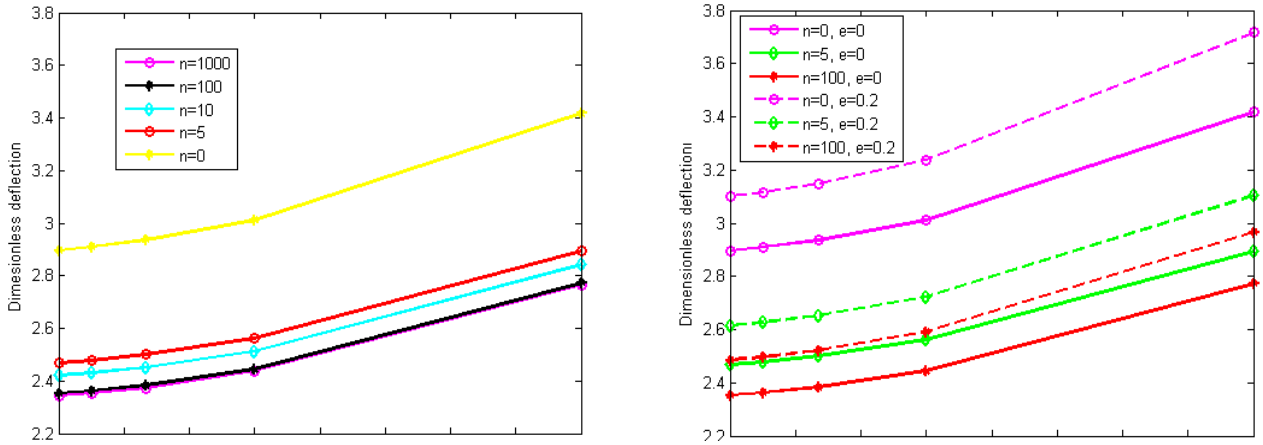

(a) $T = 300$ K, $e = 0$ (b) $T = 300$ K, $e = 0, 0.2$

Figure 6. Influence of n and thickness t on the dimensionless deflections of a fully clamped ZrO_2/SUS304 circular plate.

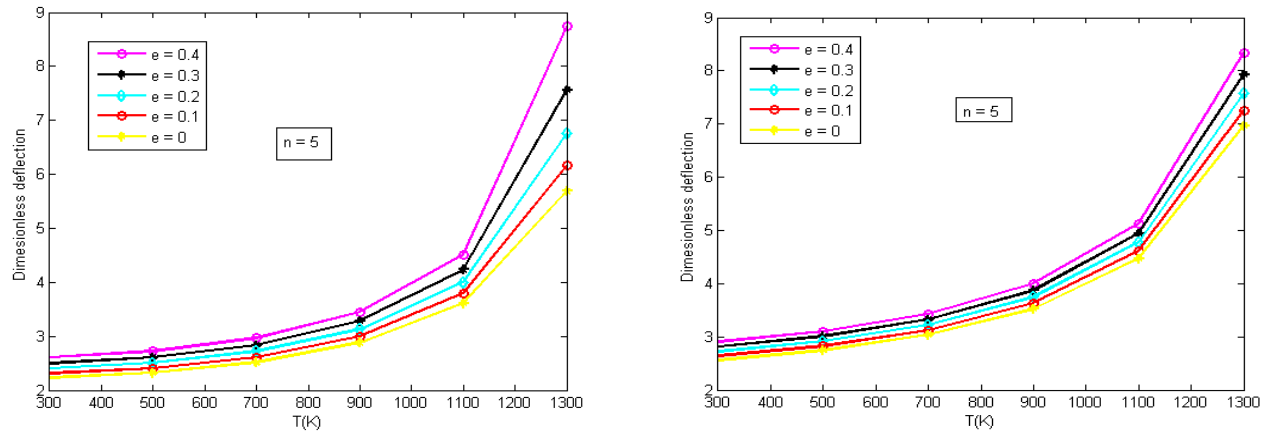

(a) $t = R/10$, $n = 5$ (b) $t = R/10$, $n = 5$

Figure 7. Influence of e on the dimensionless deflections of a fully clamped Si_3N_4/SUS304 or ZrO_2/SUS304 circular plate.

Finally, the influence of the uneven porosity distribution on the bending behavior of porous functionally graded circular plates is given. This plate made of Si_3N_4/SUS304 or ZrO_2/SUS304 with $R/t = 10$ and $n = 5$, upholding the high temperature conditions from $T = 300$ K up to 1300 K, respectively. The normalized deflections of the fully clamped plate are depicted again in Figure 7. It is clear that these values increase when e increases for both kinds of materials.

4. CONCLUSIONS

Based on a C^0-HSDT form related to Shi's third-order shear deformation theory, the paper presents a finite element analysis of porous functionally graded circular plates in a thermal environment. This study examines the impact of porosity within the structure on the deflection value. The effective characteristics were considered to be temperature-dependent when conducting numerical analysis. Furthermore, the C^0-HSDT model provided results without needing shear-correct factors. It is also noticed that this element associated with the C^0-HSDT only uses bilinear function approximations and does not require a high computational cost. The computational accuracy of this procedure is verified by comparing the obtained results with the results in other literature. The effects of various parameters on deflections are discussed. In general. the paper helps to supplement the knowledge of engineers in design.

ACKNOWLEDGEMENT AND FUNDING

The authors receive no financial support for the research, authorship, and publication of this article.

DECLARATION OF CONFLICTING INTERESTS

The authors declare no potential conflicts of interest with respect to the research and publication of this article.

REFERENCES

[1] N. Wattanasakulpong, G. B. Prusty and D. W. Kelly, Free and forced vibration analysis using improved third-order shear deformation theory for functionally graded plates under high temperature loading, *Journal of Sandwich Structures & Materials,* 15, 2013, 583-606.

[2] N. Wattanasakulpong, B. Gangadhara Prusty and D. W. Kelly, Thermal buckling and elastic vibration of third-order shear deformable functionally graded beams, *International Journal of Mechanical Sciences,* 53, 2011, 734-743.
[3] X. -L. Huang and H. -S. Shen, Nonlinear vibration and dynamic response of functionally graded plates in thermal environments, *International Journal of Solids and Structures,* 41, 2004, 2403-2427.
[4] J. Yang and H. S. Shen, Nonlinear bending analysis of shear deformable functionally graded plates subjected to thermo-mechanical loads under various boundary conditions, *Composites Part B: Engineering,* 34, 2003, 103-115.
[5] G. Shi, A new simple third-order shear deformation theory of plates, *International Journal of Solids and Structures,* 44, 2007, 4399-4417.
[6] M. D. Demirbas, Thermal stress analysis of functionally graded plates with temperature-dependent material properties using theory of elasticity, *Composites Part B: Engineering,* 131, 2017, 100-124.
[7] H. Nourmohammadi and B. Behjat, Geometrically nonlinear analysis of functionally graded piezoelectric plate using mesh-free RPIM, *Engineering Analysis with Boundary Elements,* 99, 2019, 131-141.
[8] G. Taj and A. Chakrabarti, Static and dynamic analysis of functionally graded skew plates, *Journal of Engineering Mechanics,* 139, 2013, 848-857.
[9] M. Janghorban and A. Zare, Thermal effect on free vibration analysis of functionally graded arbitrary straight-sided plates with different cutouts, *Latin American Journal of Solids and Structures,* 8, 2011, 245-257.
[10] H. Parandvar and M. Farid, Large amplitude vibration of FGM plates in thermal environment subjected to simultaneously static pressure and harmonic force using multimodal FEM, *Composite Structures,* 141, 2016, 163-171.
[11] H. L. Ton-That, Finite element analysis of functionally graded skew plates in thermal environment based on the new third-order shear deformation theory, *Journal of Applied and Computational Mechanics,* 6, 2020, 1044-1057.
[12] M. Bayat, I. M. Alarifi, A. A. Khalili, T. M. A. A. El-Bagory, H. M. Nguyen and A. Asadi, Thermo-mechanical contact problems and elastic behaviour of single and double sides functionally graded brake disks with temperature-dependent material properties, *Scientific Reports,* 9, 2019, 15317.